Journal Pre-proof

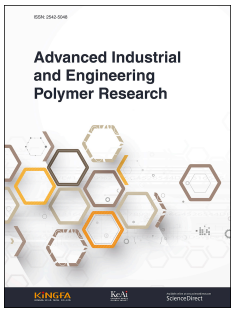

Magnetic-Responsive Triple Shape Memory Polymer from Bio-Based Benzoxazine/ Urethane Polymer Alloys with Iron Oxide Nanoparticles

Kullanard Ruenpanya, Phattarin Mora, Panagiotis Karagiannidis, Kittipon Bunyanuwat, Sarawut Rimdusit

PII: S2542-5048(24)00033-2

DOI: https://doi.org/10.1016/j.aiepr.2024.07.001

Reference: AIEPR 188

To appear in: *Advanced Industrial and Engineering Polymer Research*

Received Date: 14 May 2024

Revised Date: 29 June 2024

Accepted Date: 19 July 2024

Please cite this article as: K. Ruenpanya, P. Mora, P. Karagiannidis, K. Bunyanuwat, S. Rimdusit, Magnetic-Responsive Triple Shape Memory Polymer from Bio-Based Benzoxazine/Urethane Polymer Alloys with Iron Oxide Nanoparticles, *Advanced Industrial and Engineering Polymer Research*, https://doi.org/10.1016/j.aiepr.2024.07.001.

Magnetic-Responsive Triple Shape Memory Polymer from Bio-Based Benzoxazine/Urethane Polymer Alloys with Iron Oxide Nanoparticles

Kullanard Ruenpanya[1], Phattarin Mora[2], Panagiotis Karagiannidis[3], Kittipon Bunyanuwat[1] and Sarawut Rimdusit[1*]

[1]Center of Excellence in Polymeric Materials for Medical Practice Devices, Department of Chemical Engineering, Faculty of Engineering, Chulalongkorn University, Bangkok, 10330, Thailand

[2]Department of Chemical Engineering, Faculty of Engineering, Srinakharinwirot University, Nakhonnayok, 26120, Thailand

[3]School of Engineering, Faculty of Technology, University of Sunderland, Sunderland, SR6 0DD, United Kingdom

* Correspondence: sarawut.r@chula.ac.th; Tel.: +66-2218-6862

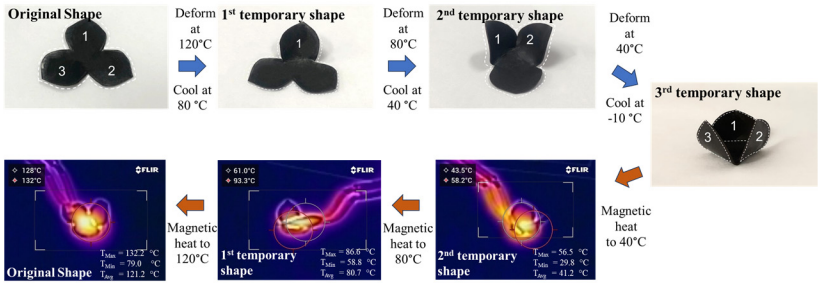

Triple shape memory behavior of V-fa/PU polymer alloys containing Fe_3O_4 NPs

Magnetic-Responsive Triple Shape Memory Polymer from Bio-Based Benzoxazine/Urethane Polymer Alloys with Iron Oxide Nanoparticles

Abstract

Novel magnetic-responsive triple shape memory polymers (SMPs) derived from bio-based benzoxazine-urethane (V-fa/PU) polymer alloys containing iron oxide nanoparticles (Fe_3O_4 NPs) were developed in this work. Shape memory effect and curing behavior of the alloys were investigated at various bio-based PU contents. The polymerization of V-fa/PU polymer alloys with a heterogeneous network generated a broad glass transition temperature, which is a crucial feature for the development of triple SMPs. The influence of Fe_3O_4 NPs incorporation into the polymer nanocomposites on the SMP performance triggered by magnetic fields was also investigated. It was found that the addition of Fe_3O_4 NPs can enhance the dynamic mechanical properties and magnetic characteristics of the V-fa/PU polymer alloys thanks to the superparamagnetic property of Fe_3O_4 NPs. Moreover, the performance of the SMPs based on V-fa/PU polymer nanocomposites filled with Fe_3O_4 NPs showed high shape fixity of up to 98%, a shape recovery of 98%, and a recovering time of 8 s. Furthermore, bio-based V-fa/PU polymer alloys containing Fe_3O_4 NPs were developed as magnetic responsive triple SMPs with shape fixity in the range of 95–97% and shape recovery in the range of 85–95%. The results suggested that magnetic responsive triple SMPs from bio-based V-fa/PU polymer alloys filled with Fe_3O_4 NPs are promising candidate for advanced applications.

Keywords : Triple shape memory polymers; Bio-based polymers; Polybenzoxazine; Urethane; Magnetic field

1. Introduction

The manufacturing of environmentally friendly products that derive from biobased materials has recently gained interest due to environmental concerns. Among the new bio-based materials being developed, smart materials derived from shape memory polymers (SMPs) have demonstrated great promise for industrial, structural, aerospace and biomedical applications [1-9].

Natural resource-based polybenzoxazines are currently researched as a stable network segment in thermosetting SMPs with excellent shape memory properties [10, 11]. The bio-based benzoxazine demonstrated exceptional mechanical characteristics, thermal stability, and SMP performance, in addition to its simple polymerization process of benzoxazine monomers [12, 13]. The bio-based SMPs reported, are triggered by various external stimuli, such as heat [11], light [14-16] and magnetic field [1]. Hombunma *et al.* (2019) have proposed heat-responsive dual SMPs from a novel bio-based benzoxazine/epoxy copolymers. They suggested that SMP made by vanillin-furfurylamine-containing benzoxazine copolymerized with epoxidized castor oil possessed good shape memory performance. Srisaard *et al.* (2021) [15] have continuously developed a near-infrared (NIR) light triggered dual SMPs based on bio-based benzoxazine/epoxy copolymer by the addition of graphene nanoplatelets (GNPs). They proposed that the photothermal fillers incorporation of GNPs into the copolymer could effectively exhibited NIR induced SMP effect.

Magnetic sensitive SMPs are mechanically functional materials that can return to their original shape following significant deformation caused by a magnetic field stimulus. They demonstrated the ability to regain a predetermined form by remote heating using magnetic nanoparticles embedded in the polymer matrix and subjected to an alternating magnetic field [17-19]. They are non-toxic to organisms and are widely used in a range of medical devices, including minimally invasive surgical techniques. The materials are transplanted into the human body and

activated in vitro by a magnetic field, where they recover their previous shape and function [20-22]. To enable magnetic field-based actuators, magnetic nanoparticles can be added into SMPs. Iron oxide nanoparticles (Fe_3O_4 NPs) are a widely utilized filler in the production of magnetic-responsive SMPs [1, 23]. Leungpuangkaew *et al.* (2023) [1] developed magnetic- and light-responsive dual SMPs from Fe_3O_4 NPs filled bio-based benzoxazine/epoxy nanocomposites. They suggested that the addition of Fe_3O_4 NPs in the range of 0-5 wt% into the nanocomposites could significantly improve SMP performance i.e., shape fixity (R_f) and shape recovery (R_N) up to 93% and 98%, respectively. Mirasadi et al. (2024) [23] have also proposed magneto-thermal dual SMP derived from PETG–ABS–Fe_3O_4 nanocomposites. Their results revealed that the SMP effect was improved by the addition of Fe_3O_4 providing potential uses for 4D printing.

Furthermore, research has suggested that polymers possessing a wide range of thermomechanical transition temperatures may exhibit a triple shape memory effect; they can take and recover up to three shapes [24-28]. Prathumrat *et al.* (2018) [29] have developed heat-responsive multiple-thermoset SMP derived from petroleum-based materials i.e., aniline based benzoxazine (BA-a) and PU. They suggested that the BA-a/PU alloys having broad T_g can be shaped into two temporary shapes with high SMP performance.

Therefore, in this work, a novel magnetic-responsive triple SMPs made entirely of bio-based benzoxazine/urethane polymer alloys incorporated by Fe_3O_4 NPs were developed. Bio-based raw ingredients, such as vanillin, furfurylamine, paraformaldehyde, and bio-based urethane, were used to create the polymer alloys. It was investigated SMP performance and curing behavior of the polymer alloys were affected by the amount of PU present. Additionally, different amounts of Fe_3O_4 NPs were added to the polymer alloys to enable their ability to respond to magnetic fields. The mechanical response to a magnetic field and their triple shape memory characteristics under magnetic field stimulation of the developed bio-based SMP nanocomposites were also examined.

2. Materials and Preparation

2.1 Material

The suppliers of furfurylamine (>99%) and vanillin (99%) were Sigma-Aldrich Pte. Ltd. (Singapore). Merck Co., Ltd. (Darmstadt, Germany) provided the paraformaldehyde (AR grade). Siripanit Industry Co., Ltd. (Thailand) provided the castor oil polyol having viscosity of 2,500-3,200 mPa•s and hydroxyl number of 110-120 mg KOH/g. The Vencorex (Thailand) Co., Ltd. provided kind support for 2,4-toluene diisocyanate (TDI). Fe_3O_4 nanoparticles (97%) with a diameter ranging from 50-100 nm, bulk density of 4.8-5.1 g/cm^3, a surface area of approximately 6-8 m^2/g and thermal conductivity of 4-8 W/m•K were acquired from Sigma-Aldrich Pte. Ltd. located in St. Louis, MO, USA. All chemicals were used as received.

2.2 Preparation of benzoxazine resin

Benzoxazine resin (V-fa) was produced using vanillin, furfurylamine, and paraformaldehyde according to the solventless method with no further removing of solvent [30]. The reactants were combined at a ratio of 1:1:2 and stirred for 1 h at 105 °C to induce the Mannich-like condensation without using of catalyst. After the reaction mixture was cooled to room temperature, a transparent yellow monomer product was produced. The synthesized V-fa was utilized in the manufacture of the benzoxazine/urethane alloys subsequent stage.

Castor oil polyol and 2,4-toluene diisocyanate (TDI) were combined at a molar ratio of 1:2 to produce urethane prepolymer (PU). The two reactants were combined at 70 °C with a nitrogen purge in a round-bottom flask with five necks. The liquid PU was stored in a closed container with nitrogen gas purged and allowed to cool to ambient temperature before being kept in a refrigerator.

2.3 Preparation of benzoxazine/urethane alloys filled with Fe_3O_4 NPs

Benzoxazine/urethane alloys (V-fa/PU alloys) were synthesized by mixing V-fa with PU at the appropriated ratio. The Fe_3O_4 NPs were kept in a desiccator at room temperature after being dried at 80°C for 24 h in an air-circulated oven until a consistent weight was reached. Then, to create a well-dispersed mold, different amounts (i.e., 0, 1, 3, 5, 7 and 10 wt%) of the Fe_3O_4 NPs were mixed into the PU at room temperature for 24 h. This was followed by a gentle mixing with V-fa resin at 105 °C under stirring until a homogeneous mixture was obtained and poured into an aluminum mold. The samples were step-cured in an oven at 130 °C for 1 h, 140 °C for 1 h, 150 °C for 1 h and 160 °C for 1 h, respectively. Finally, the samples were cooled down to room temperature to obtain V-fa/PU alloys filled with Fe_3O_4 NPs.

2.4 Sample characterization

The molecular properties and network formation of each sample were investigated with a Perkin Elmer spectrum GX FT-IR spectrometer with an ATR attachment (Waltham, MA, USA). The specimen surface was placed onto a flat diamond crystal IRE with a 1.5 mm sampling diameter in order to get an infrared spectrum. Using a pressure apparatus, the specimen was forced up against the flat diamond crystal until the maximum pressure that could be achieved was reached. All spectra were collected as a function of time using 32 scans with a resolution of 4 cm^{-1} and a wavenumber range of 4000 to 400 cm^{-1}.

A dynamic mechanical analyzer (DMA) model DMA242 from Netzsch, Inc. (Bavaria, Germany) was used to study dynamic mechanical properties. The samples were test under tension mode with dimensions of 20 ×5 ×0.3 mm^3 at a frequency of 1 Hz and a strain amplitude of 10 μm. Heating rate was 2 °C/min from -100 °C to 200 °C under air atmosphere. Gage length of the

samples was measured to be approximately 10 mm. The storage modulus (E'), and loss tangent (tan δ) of the samples were measured. The local maxima of the loss tangent curves were used to determine the glass transition temperature (T_g).

A thermogravimetric analyzer (Mettler Toledo, model TGA1 Module, Thailand) was used to examine the thermal stability of samples with varying amounts of Fe_3O_4 NPs. The specimens were analyzed under a nitrogen atmosphere at flow rate of 50 mL/min from 25 to 800 °C with a heating rate of 20 °C/min. Every specimen was put in a crucible with a notional mass of 5-10 mg. The degradation temperature at 5% weight loss (T_{d5}) and residual weight at 800°C of the sample were determined.

The morphology and dispersion of Fe_3O_4 NPs in the polymer matrix was investigated by scanning electron microscope (SEM, model JSM-6510A from JEOL Ltd., Tokyo Japan) using an acceleration voltage of 15 kV. All specimens were coated with a thin layer of gold using a JEOL ion sputtering device (model JFC-1200).

A vibrating sample magnetometer (VSM, Lakeshore 7404) was used to measure the sample's magnetization curves while it was at room temperature. The magnetic field's range was between -10000 and 10000 Oe.

Shape fixity of the specimen under bending load were programed as shown in Fig. 1(a) – Fig. 1(c). In the first step, the specimens having dimensions of 30 ×3 ×0.3 mm^3 (Fig 1(a)) were heated to T_g+20°C while being bent at a 90° angle to form first temporary V shape (Fig 1(b)). In the second step, the specimen was then cooled to T_g-20°C while being bent at a 180° angle to form second temporary U shape (Fig 1(c)). After that, the specimen was cooled to room temperature while applying load; the bending force was then eliminated. The specimen was recovered with a

magnetic field at the bending point to initiate the shape recovery procedure as shown in Fig 1(d) – Fig 1(f). A digital camera was used to record the shape recovery procedure.

The deflection after unloading was then measured and the shape fixity of each sample was determined according to Eq. (1)

$$R_f = (\theta_F/\ \theta_0) \times 100\% \quad (1)$$

Where: θ_0 is the original storage angle, θ_F is the angle of the tested sample at the fix state

In the shape recovery process, the sample was placed into an alternating magnetic field at a frequency of 750-1150 kHz (Inductive Heating Machine). The fixed shape was subsequently recovered. The shape recovery values were calculated by Eq. (2).

$$R_N = (\theta_R/\ \theta_0) \times 100\% \qquad (N = 1, 2, 3, \ldots) \quad (2)$$

Where R_N represents the shape recovery ratio of the N^{th} thermo-mechanical bending cycle obtained through Eq. (2).

θ_R is the angle of the tested sample at the recovery state.

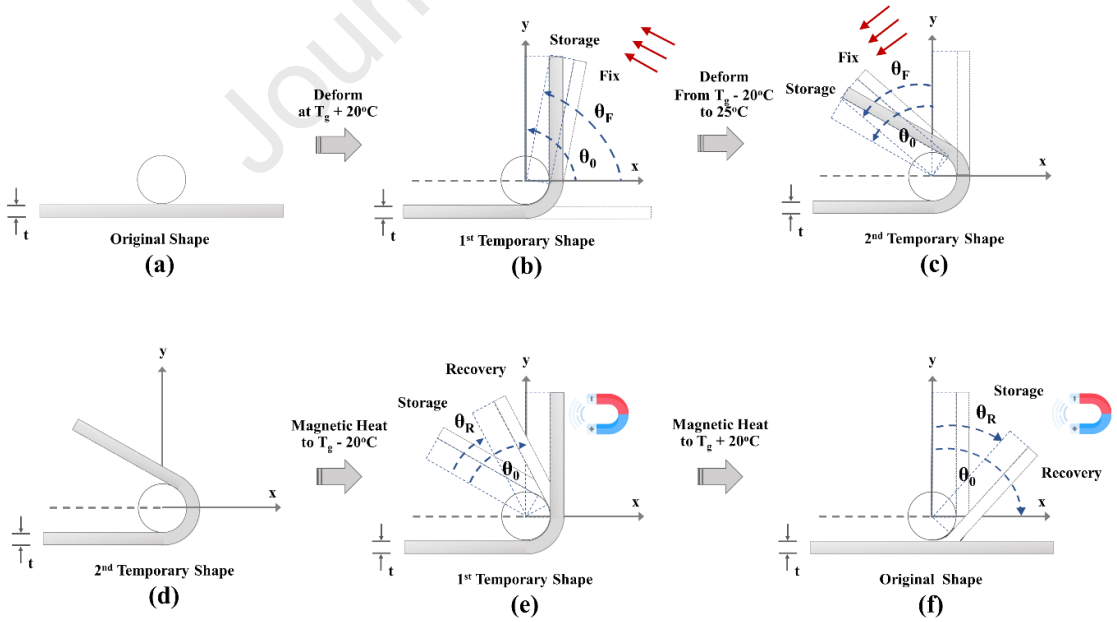

Fig. 1 Scheme of the programming for triple shape memory performance test.

3. Results and discussion

3.1 Network formation of V-fa/PU mixture and V-fa/PU polymer alloys

The structure of the monomers and network formation of V-fa/PU polymer alloys were investigated by FT-IR technique. Fig. 2 depicts the FT-IR spectra of a V-fa resin, a castor oil polyol-based PU, V-fa/PU mixture and V-fa/PU polymer alloys. From Fig. 2(a), the absorption peaks of V-fa monomer assigned to C-O-C of the oxazine ring were found at 905, 923 and 1229 cm^{-1} [31]. The IR absorption peaks at 760, 997, and 1583 cm^{-1} validated the furan group of V-fa monomer [31]. The IR absorption peak at 1686 cm^{-1} verified the carbonyl (C=O) group of vanillin [32]. The spectra also revealed a peak at 1364 cm^{-1} that corresponds to the tetra-substituted benzene ring of the V-fa monomer [31]. In the case of castor oil polyol-based urethane prepolymer, as shown in Fig. 2(b), the characteristic IR absorption peak at 1736 cm^{-1} represented the C=O fatty acid ester group of the polyol, while the peaks at 1532 and 2276 cm^{-1} represented the urethane group and free isocyanate (N=C=O) group, respectively. These peaks demonstrated that the urethane prepolymer and V-fa monomer had been successfully synthesized [33, 34], which are ready for further polymer alloy preparation.

The network formation of the uncured V-fa/PU mixture compared to the cured V-fa/PU polymer alloy was studied as shown in Fig. 2(c) and Fig. 2(d), respectively. Regarding the polymerization of the V-fa/PU mixture, the reaction starts with the thermally accelerated ring-opening polymerization of the benzoxazine resin, resulting in the release of a free hydroxyl group. The free hydroxyl group of polybenzoxazine generated then interacts with the free isocyanate group of the urethane prepolymer, causing urethane linkages (-NH-CO-O) [35, 36]. The disappearance of the absorption bands at 905, 933, and 1229 cm^{-1} corresponding to the oxazine ring of V-fa, the disappearance of the isocyanate peak at 2276 cm^{-1}, and the decrease in intensity

of the hydroxyl group peaks around 3200-3550 cm^{-1} suggest that the isocyanate of urethane prepolymer and hydroxyl group of polybenzoxazine have been consumed. The results suggested that the V-fa/PU polymer alloys generated via a chemical crosslinking network were successful.

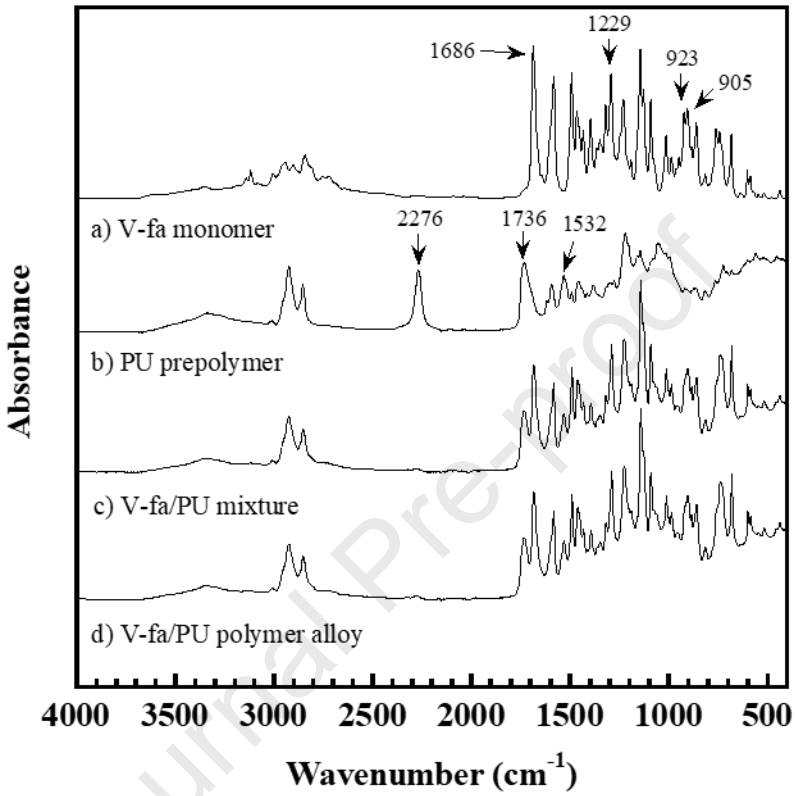

Fig. 2. FT-IR spectra of (a) V-fa monomer, (b) bio-based PU, (c) V-fa/PU binary mixture and (d) V-fa/PU polymer alloy.

Fig. 3 depicts a potential chemical reaction between the PU prepolymer and the V-fa monomer. Theoretically, heating at an appropriate curing temperature opened the V-fa oxazine ring (Fig. 3(a)). As shown in Fig. 3(b), the hydrogen-bonded urethane carbonyl linkages in the polymer alloy networks were created by the reaction between the isocyanate group of the urethane prepolymer and the phenolic hydroxyl groups of the ring opened polybenzoxazine (poly(V-fa)). Additionally, these outcomes correlate well with earlier reports by Mora *et al.* [37] and Parnklang *et al.* [34].

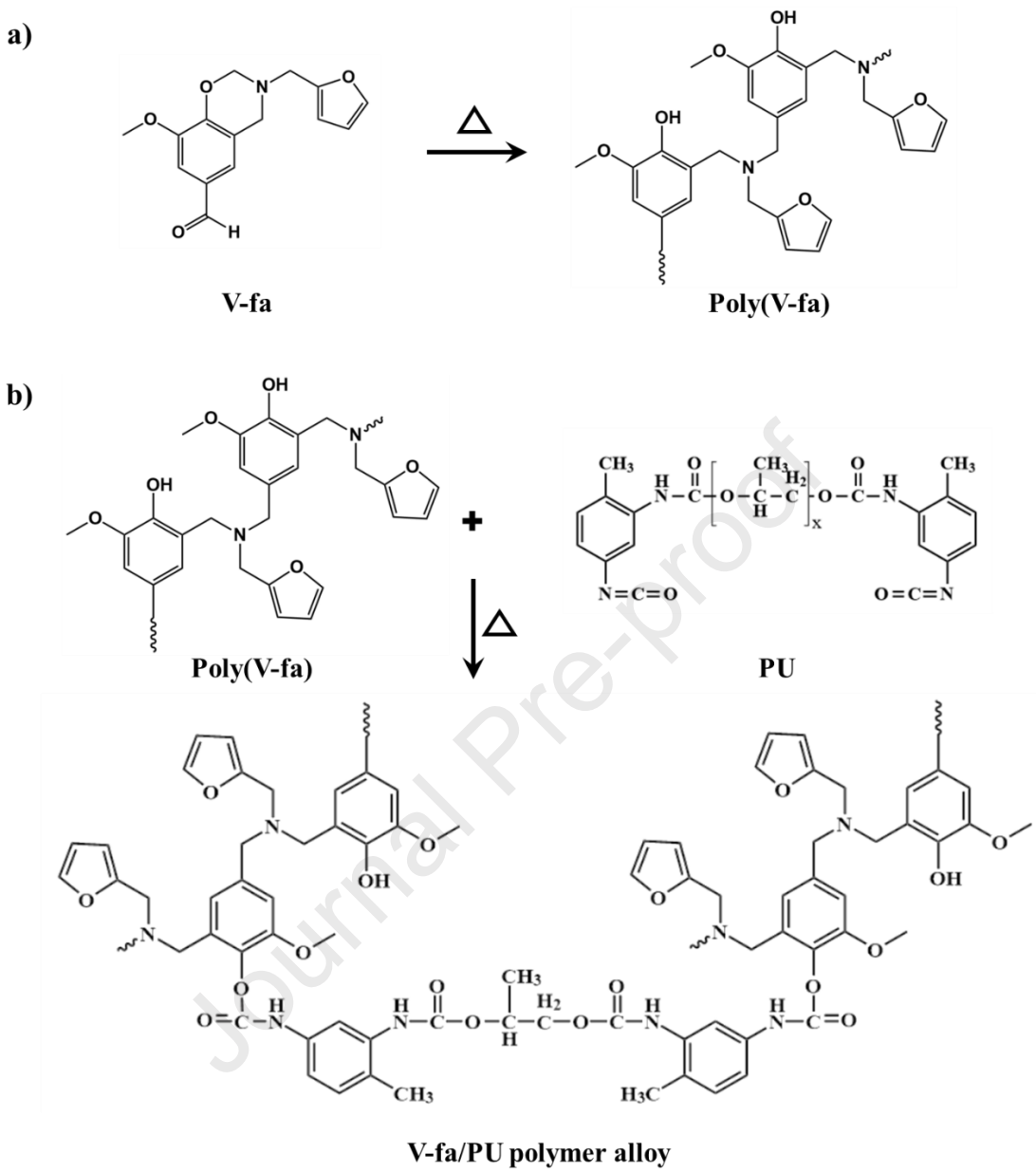

Fig. 3. (a) Curing reaction of V-fa monomer and (b) A possible chemical reaction between poly(V-fa) and bio-based PU.

3.2 Dynamic mechanical properties of V-fa/PU polymer alloys at various PU Content

Utilizing dynamic mechanical analysis (DMA), the dynamic mechanical properties of benzoxazine–urethane polymer alloys with varying PU concentrations were examined. One of the most important parameters for improving shape fixity performance is specimen stiffness, which is related to the storage modulus. Fig. 4 illustrates the storage modulus at glassy state (-100 °C) of V-fa/PU polymer alloys which was determined to be 2.34, 2.12, 1.86, 1.42, and 1.13 GPa with the addition of PU at 40, 50, 60, 70, and 80 wt%, respectively. The decrease in storage modulus at the glassy state of polymer alloys with increasing PU content can be attributed to the more flexible structure of castor oil polyol-based PU compared to V-fa, which supplied more flexibility to the developed polymer alloys [38].

T_g of the specimens which is one of the most important variables under programming SMPs was determined from the maxima tan δ peak as also shown in Fig. 4. The T_g of V-fa/PU polymer alloys were substantially decreased i.e. 60, 57, 51 and 47^{o}C with increasing PU content i.e. 40, 50, 60, and 70 wt%, respectively. T_gs of V-fa/PU polymer alloy tended to decrease with increasing PU mass concentrations due to the polymer network flexibility contributed by soft chain of PU [38]. Furthermore, the results demonstrated that the T_g of V-fa/PU polymer alloys with PU content ranging from 40-70 wt% displayed two broad, separate peaks, indicating that the V-fa/PU polymer alloys possessed a heterogeneous network. The heterogeneous network of the V-fa/PU polymer alloys plays a key influence in its microstructure and performance, which may account for its broad glass transition range [39]. Due to the lower degree of phase separation between benzoxazine and urethane, the V-fa/PU sample with a 20/80 mass fraction only shows a single peak with a T_g value of around 11 °C. Also, as the amount of V-fa in the system increased, the T_g of the alloy was also

increased. This was because the polybenzoxazine and urethane had a much stiffer conjugated structure and a heavily crosslinked network [29].

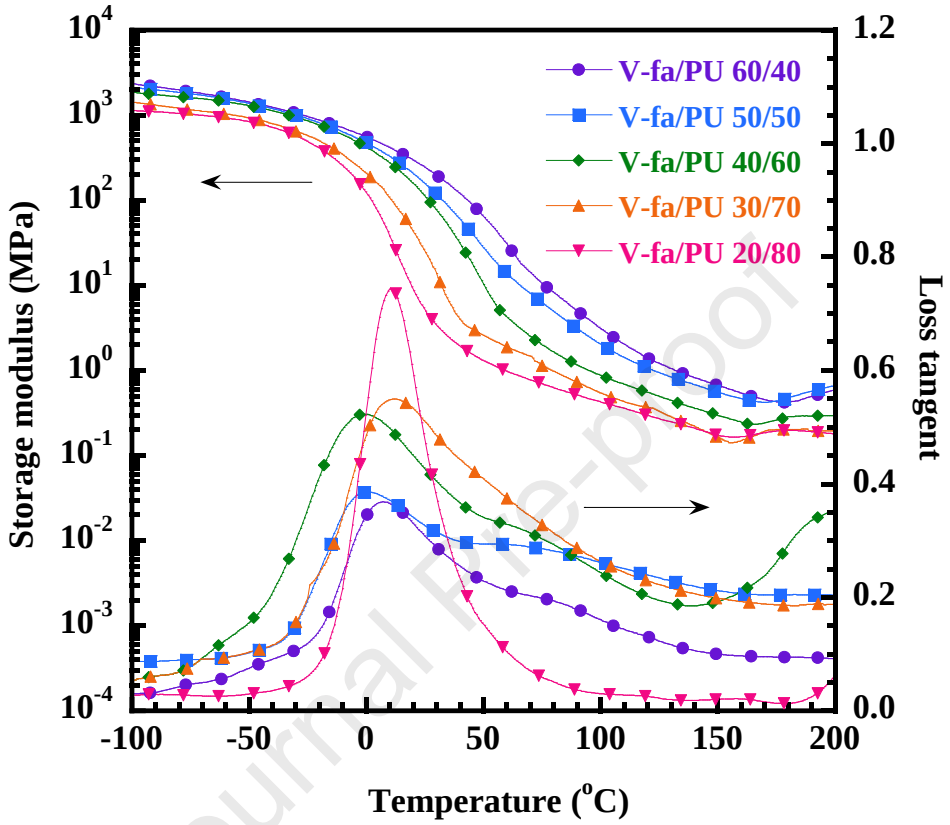

Fig. 4. Dynamic mechanical properties of V-fa/PU at various PU Content.

3.3 Shape Memory Performance of V-fa/PU polymer alloys as various PU content

The performance of a specific heat-responsive SMP system was determined and programed as shown in Fig. 5. According to Eq. (1) and Eq. (2), the shape fixity and shape recovery ratio were computed, respectively. The shape fixity parameter specifies the capacity to fix a structure into a temporary shape while the shape recovery ratio expresses the ability of the structure to return to each original shape. Table 1 displays the shape fixity and shape recovery characteristics of V-fa/PU polymer alloys. The value of shape fixity of V-fa/PU polymer alloys was increased with

decreasing PU content. When PU contents decrease, the increasing storage modulus of V-fa/PU polymer alloys at glassy state reflected to low cohesive energy and an optimum propensity for creep associated to shape change [34, 40]. As a result, shape fixity values increased as the PU content decreased.

The shape recovery values decreased with decreasing the PU concentration. It was caused by the fact that PU has a more flexible chain than V-fa and that heat can cause V-fa/PU polymer alloys to recover its shape. Entropy-driven shape recovery is achieved via coordinated movements of net-points and chain segments, and a bulky substituent might inhibit chain conformation changes for deformation specimens under motion restrictions [41]. The findings indicates that V-fa/PU polymer alloys with a 40% PU content demonstrated an excellent balance of shape memory performance and the broadest thermomechanical transition temperature, which is a crucial feature for additional triple-shape memory properties.

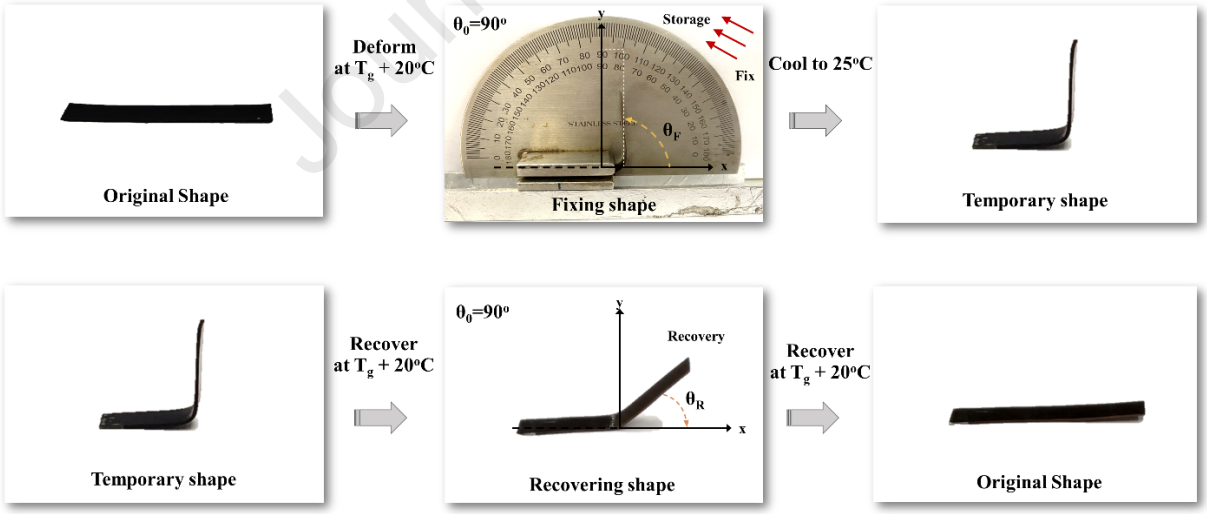

Fig. 5. Programming for heat-responsive shape memory performance test of V -fa/PU polymer alloys.

Table 1. Shape memory performance of V -fa/PU polymer alloys at various V-fa contents.

Sample type	Shape Fixity, R_f (%)	Shape Recovery, R_N (%)	Recovering time (s)
V-fa/PU (20/80)	68 ± 1.4	100 ± 0.0	8 ± 0.71
V-fa/PU (30/70)	78 ± 0.2	100 ± 0.0	13 ± 1.6
V-fa/PU (40/60)	85 ± 1.1	100 ± 0.0	17 ± 2.1
V-fa/PU (50/50)	93 ± 1.4	98 ± 0.8	26 ± 1.9
V-fa/PU (60/40)	96 ± 0.6	94 ± 1.0	30 ± 2.6

3.4 Magnetic property of V-fa/PU at various Fe_3O_4 NPs Content

Using a VSM, the magnetic characteristics of V-fa/PU polymer alloys loaded with Fe_3O_4 NPs at room temperature were analyzed. Fig. 6 depicts the isotherms of magnetization (M) with applied magnetic field (H, from -10000 to 10000 Oe) for V-fa/PU polymer alloys containing Fe_3O_4 NPs (1-10wt%) and pure Fe_3O_4 NPs. According to the magnetometer, pure Fe_3O_4 nanoparticles have a saturation magnetization of 89.3 emu/g as shown in inserted figure. The saturation magnetization of V-fa/PU polymer alloys containing 1, 3, 5, 7, and 10 wt% Fe_3O_4 nanoparticles increased to be 0.8, 2.5, 3.3, 4.9, and 7.0 emu/g, respectively. The increased mobility of the Fe_3O_4 NPs made it easier for them to move in the direction of the magnetic field. The saturation magnetization increased as a result [42].

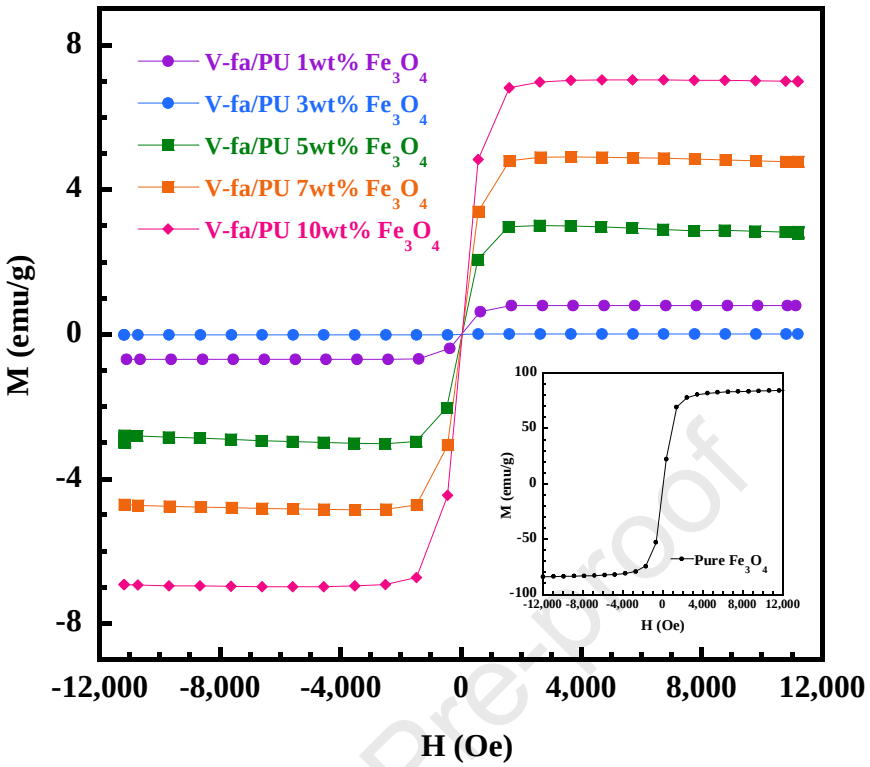

Fig. 6. Magnetization curves of pure Fe_3O_4 NPs and V-fa/PU polymer alloys at 60/40 wt% containing different contents of Fe_3O_4 NPs.

3.5 Molecular information of V-fa/PU polymer alloys filled with Fe_3O_4 NPs

FT-IR spectra were collected from V-fa/PU polymer alloys filled with Fe3O4 NPs and are presented in Fig. 7. The FT-IR spectra of pure Fe_3O_4 nanoparticles exhibited an absorption band at 547 cm^{-1}, which is remarkably equivalent to the finding reported by Kim *et al.* [43]. The addition of Fe_3O_4 nanoparticles to V-fa/PU polymer alloys caused the formation of a new absorption band at 570 cm^{-1}, linked with the stretching vibration mode of the metal-oxygen Fe-O bond in the crystalline lattice of Fe_3O_4 [44]. The intensity of an absorption band at 570 cm^{-1} tended to increase with increasing Fe_3O_4 content of the polymer alloys. This indicated the strong interaction between nanoparticles of Fe_3O_4 and the polymer matrix which can affect to further thermal properties and SMP performance. The broadened band corresponding to Fe–O in Fe_3O_4 nanoparticles suggests

that polymer chains are attached to the surface of the nanoparticles. [45]. Overall, the findings demonstrated that V-fa/PU polymer alloys containing varying concentrations of Fe_3O_4 NPs were successfully formed.

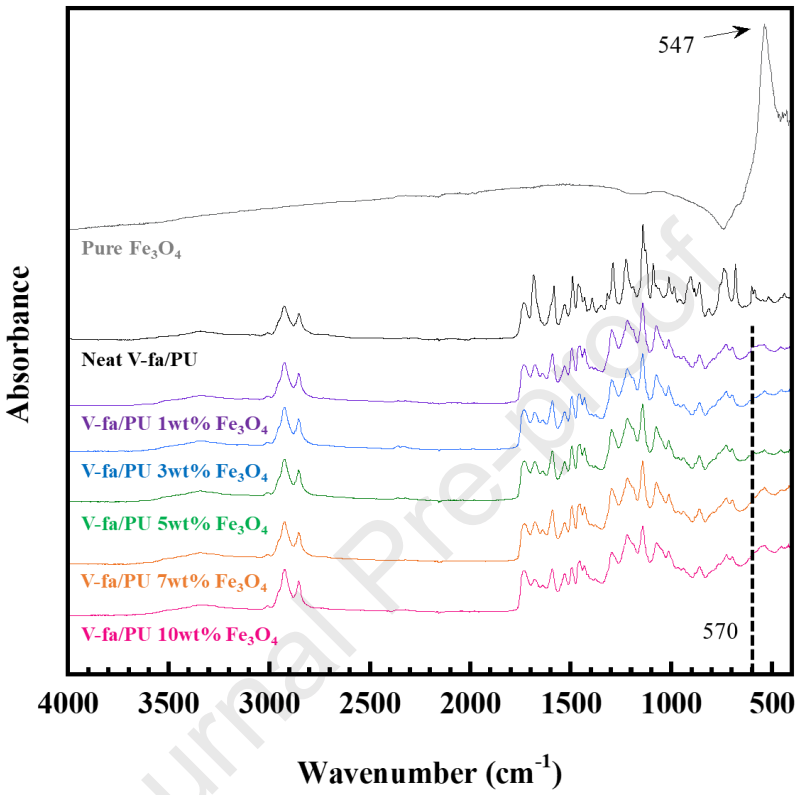

Fig. 7. FT-IR spectra of pure Fe_3O_4 NPs and V-fa/PU polymer alloys at 60/40 wt% containing different contents of Fe_3O_4 NPs.

3.6 Thermal Stability of V-fa/PU polymer alloys at various Fe_3O_4 Content

TGA was employed to determine the thermal stability of V-fa/PU polymer alloys containing Fe_3O_4 NPs (Fig. 8). The T_{d5} of V-fa/PU polymer alloys was determined to be 287 ℃. In contrast, the T_{d5} of V-fa/PU polymer alloys loaded with 1, 3, 5, 7, and 10 wt% Fe_3O_4 NPs were determined to be 290, 294, 311, 316, and 316 ° C, respectively. Furthermore, the residual weights of V-fa/PU polymer alloys containing Fe_3O_4 NPs at 1, 3, 5, 7, and 10 wt% were determined to be 41, 43, 46, 47, and 50 wt%, respectively. The good dispersion and strong interfacial adhesion

between Fe_3O_4 NPs and the polymer matrix, with polymer chains attached onto the surface of the nanoparticles, could be responsible for the increase in T_{d5} and residual weight at 800 °C in V-fa/PU filled the with Fe_3O_4 NPs [45].

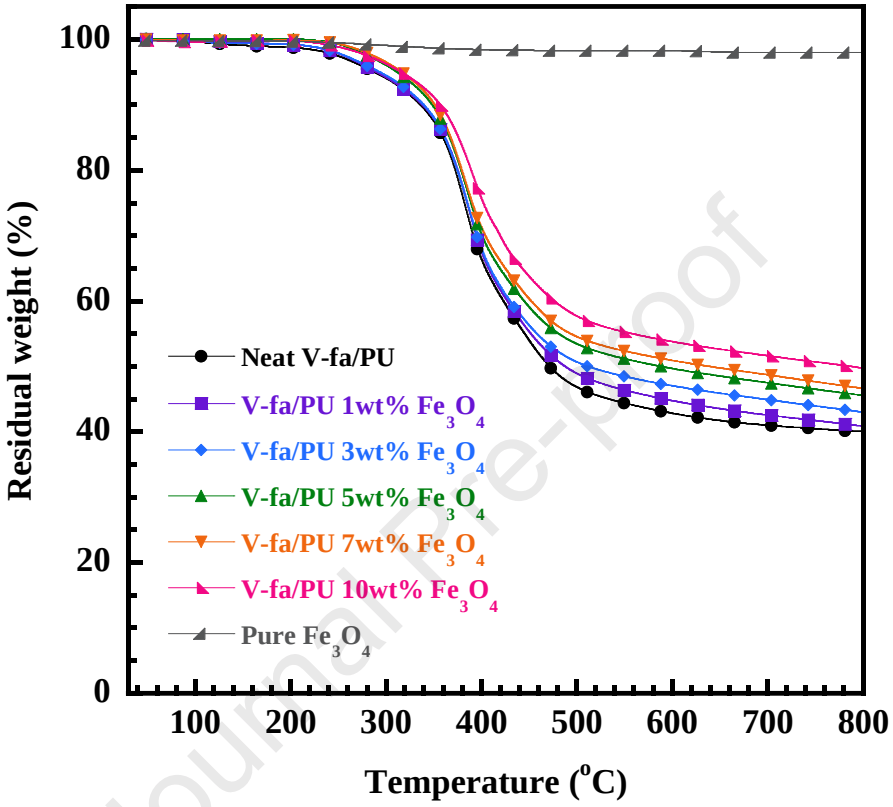

Fig. 8. TGA thermograms of pure Fe_3O_4 NPs and V-fa/PU polymer alloys at 60/40 wt% containing different content of Fe_3O_4 NPs.

3.7 Dynamic Mechanical Analysis (DMA) of V-fa/PU at various Fe_3O_4 Content

Fig. 9 illustrates the storage modulus of V-fa/PU polymer alloys with a V-fa/PU ratio of 60/40 and a loading of 1–10 wt% Fe_3O_4 NPs. The storage modulus of V-fa/PU polymer alloys loaded with Fe_3O_4 NPs was higher than that of V-fa/PU polymer alloys in a glassy state (-100 °C). This occurs as a result of the rigid Fe_3O_4 NPs increasing the stiffness of the sample, hence raising the specimen's modulus. The storage modulus of polymer alloys containing Fe_3O_4 nanoparticles

at concentrations of 1, 3, 5, 7, and 10 wt% were 2.56, 2.99, 3.41, 4.11, and 3.68 GPa, respectively. The storage modulus of the samples improved up to 7 wt% Fe_3O_4 NPs, with the value thereafter decreasing. Comparing V-fa/PU sample filled with 10 wt% Fe_3O_4 against the sample filled with 7 wt% Fe_3O_4, we find that the storage modulus of the higher Fe_3O_4 content sample reveals a relative decrease, indicating nanoparticle aggregation [46].

According to the tan δ curve, V-fa/PU polymer alloys have two peaks or two T_{gs}. The initial rise at 6 °C in the polymer alloys was entirely connected to the polyurethane part. The second peak at increased temperatures is due to alloys of copolymerized V-fa/PU polymers. The T_g of V-fa/PU polymer alloys was determined to be 60 °C. In contrast, the V-fa/PU polymer alloys incorporating Fe_3O_4 nanoparticles at 1, 3, 5, 7, and 10wt% were increased to 70, 77, 79, 98, and 87 °C, respectively. This might be because the increased Fe_3O_4 NPs concentration up to 7wt% impeded the segmental mobility of polymer alloy chains, which may have contributed to an increase in T_g. The magnetite filler agglomerating in the V-fa resin is probably to blame for the drastic fall in T_g for 10 wt% Fe_3O_4 NPs filled polymer composite.

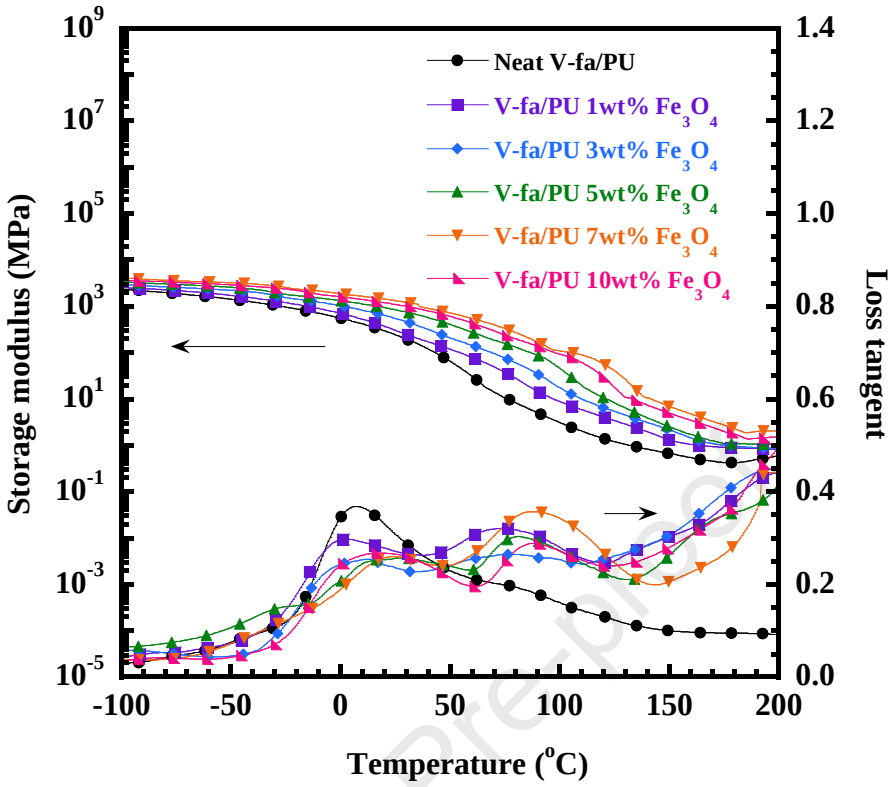

Fig. 9. Dynamic Mechanical Analysis (DMA) of V-fa/PU polymer alloys at 60/40 wt% containing different content of Fe_3O_4 NPs (1-10wt%).

3.8 Morphology and dispersion

The morphology of V-fa/PU polymer alloys loaded with Fe_3O_4 NPs was examined using scanning electron microscopy (SEM). Fig. 10 shows cross-sectional micrographs of V-fa/PU polymer alloys and V-fa/PU with various amounts of Fe_3O_4 NPs. Fig. 10(a) demonstrates that the surface of pure V-fa/PU polymer alloys is rather smooth. Fig. 10(b)–(e) show images obtained from composites with 1, 3, 5, and 7 wt% of the Fe_3O_4 NPs and reveals that Fe_3O_4 NPs were well dispersed in the matrix. On the contrary, Fig. 10(f) shows that an excessive number of nanoparticles led to agglomeration at 10 wt%. This might be the reason for the decrease in storage modulus and T_g presented in the previous DMA results.

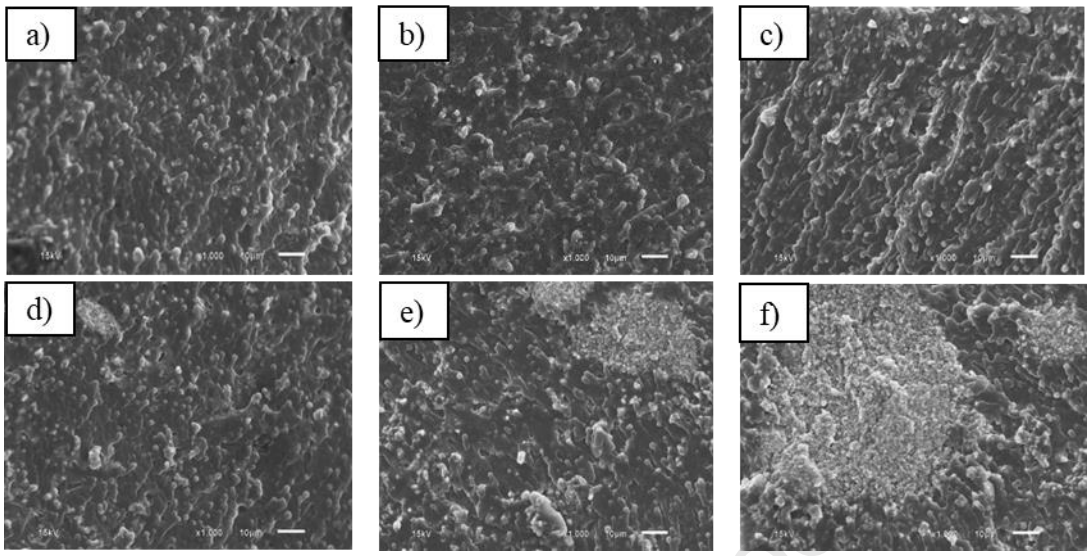

Fig. 10. SEM images of (a) neat V-fa/PU and cross section V-fa/PU at 60/40 wt% polymer alloys at various Fe_3O_4 NPs content: (b) 1 wt%, (c) 3 wt%, (d) 5 wt%, (e)7 wt%, (f) 10 wt%.

3.9 Infrared Thermographs of V-fa/PU (60/40) Polymer Alloys at Various Fe_3O_4 NPs Contents

In this study, the effect of Fe_3O_4 NPs content on recovery temperature actuated by magnetic field was investigated. The samples were then exposed to magnetic heating by the application of an alternating magnetic field (750-1150 kHz). All specimen was captured by thermal camera, when they were in temporary shape at room temperature and recover their shape into original shape at high temperature actuated by magnetic field. Fig. 11 depicts thermal images obtained from samples with different Fe_3O_4 NPs content at room temperature (left) and the corresponding images under magnetic field (right). When exposed to an external magnetic field, the shape recovery process could be done in 5 seconds. The specimen temperature of V-fa/PU 60/40 wt% polymer alloys filled with Fe_3O_4 NPs of 1 wt% was relatively low due to insufficient magnetic induced heating. However, increasing the amount of Fe_3O_4 NPs in specimens can increase heat generation and temperature from 48.6 to 77.9 ^oC, enabling the specimens to achieve the appropriate transition

temperature. The results revealed that the incorporation of Fe_3O_4 NPs could help to generate magnetic heating in the polymer alloys.

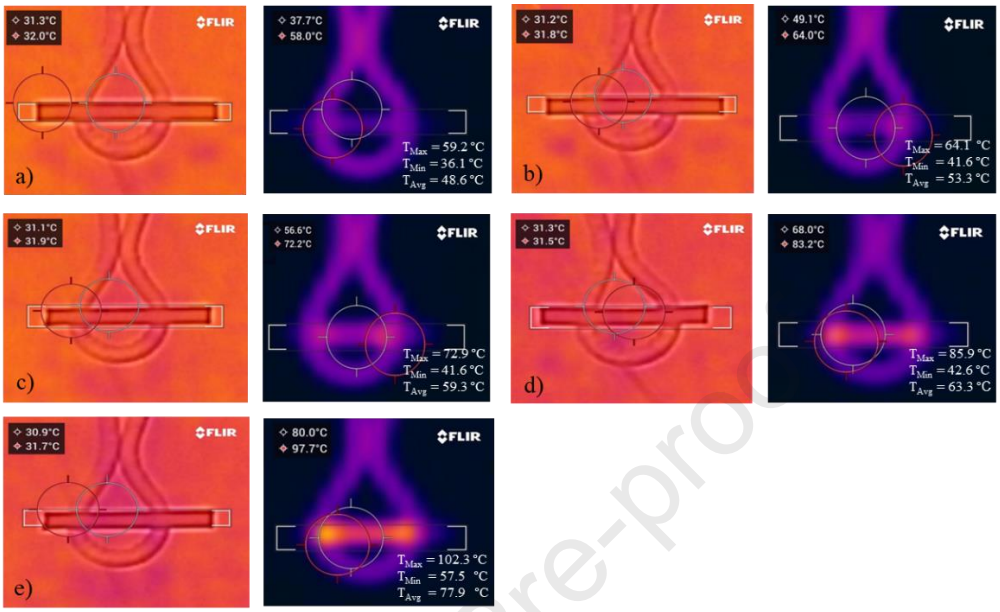

Fig. 11. Infrared Thermographs of V-fa/PU polymer alloys at 60/40 wt% containing different content of Fe_3O_4 NPs: (a) 1 wt%, (b) 3 wt%, (c) 5 wt%, (d) 7 wt% and (e) 10 wt% at room temperature (left) and under magnetic field actuation (right).

3.10 Shape Memory Performance of V-fa/PU as various Fe_3O_4 NPs content

Table 2 shows the values for shape fixity and shape recovery for V-fa/PU polymer alloys at 60/40 wt% filled with various Fe_3O_4 NPs content. The shape fixity value of neat V-fa/PU polymer alloys was around 96%. While the shape fixity values resulting from the inclusion of Fe_3O_4 NPs at concentrations of 1, 3, 5, 7, and 10 wt% were 96%, 97%, 97%, 98%, and 99%, respectively. A slight increase in shape fixity may be attributed to the presence of Fe_3O_4 nanoparticles (NPs) in composites, which improves the interaction between nanoparticles of Fe_3O_4 and the polymer matrix mentioned in previous subsection 3.5, resulting in a more rigid and stable polymer network that prevents the chains mobility, thereby increasing the shape fixity values. This

phenomenon was similar to those of previously reported with SMP based on particle-filled polymer composites systems [15, 47].

The shape recovery value of pure V-fa/PU polymer alloys was around 94%, whereas the shape recovery values of V-fa/PU polymer alloys loaded with 1,3,5,7 and 10 wt% Fe_3O_4 NPs were approximately 85%, 90%, 97%, 98%, and 99%, respectively. This is because the nanoparticles are spread out evenly and there are more physical and chemical interactions taking place inside the system. This can also be attributed to the higher magnetic absorption of the nanocomposites as a result of the increased loading of magnetically active Fe_3O_4 NPs. The nanocomposites kept their shape and returned to their initial state well over several test cycles. These results show that they could be used as advanced shape memory materials in a number of industries [45, 48]. As it is commonly known that polymers have a low thermal conductivity, improving the thermal conductivity and, consequently, the heat transfer efficiency, might improve the performance of SMPs [49].

Table 2. Shape memory performance of V-fa/PU polymer alloys at 60/40 wt% containing different content of Fe_3O_4 NPs.

Fe_3O_4 content (wt%)	Shape Fixity, R_f (%)	Shape Recovery, R_N (%)	Recovering time (s)
1	96 ± 0.9	85 ± 2.1	32 ± 0.8
3	97 ± 0.5	90 ± 1.7	21 ± 2.5
5	97 ± 0.7	97 ± 1.6	18 ± 0.7
7	98 ± 1.1	98 ± 1.1	8 ± 1.2
10	99 ± 1.3	99 ± 0.4	8 ± 1.2

3.11 Triple shape memory Properties of V-fa/PU polymer alloys at different Fe_3O_4 Content

The T_g range depicted by the onset and endset of the tan δ is a crucial variable in the triple shape memory process (Table 3). In this range of temperatures, the polymer can be temporarily changed into many different shapes. The highest V-fa content for the V-fa/PU polymer alloys was 60 wt% and was filled with 7 wt% Fe_3O_4 NPs; and it was this percentage of V-fa which showed the broadest T_g temperature range and the optimum shape memory performance.

Fig. 12 depicts the triple shape memory performance of the flower-shaped V-fa/PU (60/40) polymer alloys loaded with 7 wt% Fe_3O_4 NPs. For shape fixity process, the specimen was heated for 20 minutes at 120°C. Then, it was bent into the 1st temporary shape and cooled down to 80°C for 20 min. After that, the specimen was curved into the 2nd temporary shape and cooled down to 40°C for 20 min. Finally, the 3rd temporary shape was bent at 40 °C and cooled down to -10°C for 20 min. For the recovery process, the 3rd temporary shape changed into the 2nd temporary shape when it was heated to a temperature of 40 °C. Then, the specimen was recovered from the 2nd shape to the 1st shape at 80 °C before recovering its original shape again at 120 °C. Infrared temperature thermometer gun was used to confirm that the specimen has a temporary shape at pre-defined temperatures as also shown in Fig. 12.

Table 3. The glass transition temperatures of V-fa/PU polymer alloys at 60/40 wt% containing different contents of Fe_3O_4 NPs.

Fe_3O_4 contents	T_g (°C)	T_g range (°C)	ΔT_g (°C)
1	83	-58 to 114	172
3	85	-41 to 112	154
5	87	-73 to 128	201
7	98	-68 to 145	213
10	90	-49 to 132	181

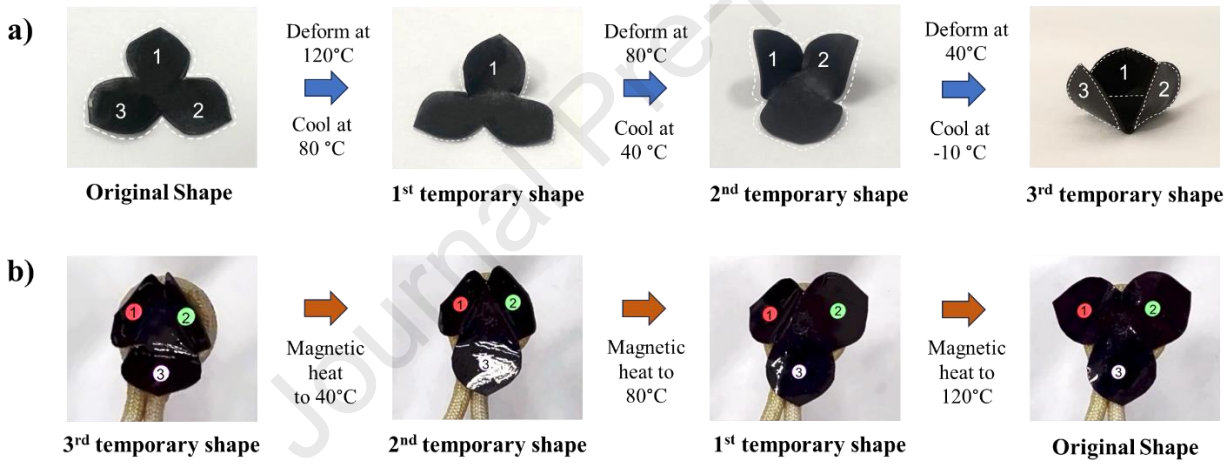

Fig. 12. Triple shape memory behavior of V-fa/PU polymer alloys at 60/40 wt% containing 7 wt% Fe_3O_4 NPs: a) thermal shape programming and b) magnetic shape recovery.

3.12 Electric Circuit Application of Triple Shape Memory Polymer

SMPs could be used as sensors and actuators in aerospace engineering, 4D printing, self-healing, electroactive SMPs, biological fields, automobile etc. [50]. In this study, a remote-controlled electric circuit in a broad temperature range was considered. Fig. 13 shows the electric circuit working with the applying triple SMP as remote bridge materials. The triple SMP acted as switch to control 3 different light bulbs working by changing its shape into 3 different shapes when triggered by heating. In the triple SMP programming step, the sample of V-fa/PU polymer alloy at 60/40 wt% containing 7 wt% Fe_3O_4 NPs was heated to approximately 120°C while being bent at a 90° angle to form 1st temporary shape. The sample was then cooled to 80°C while being bent at a 180° angle to form 2nd temporary shape followed by cooling to 40^{o}C while being twisted to form 3rd temporary V shape. The sample then is cooled to -10^{o}C and the force was then removed to obtain the programmed triple SMP. In the recovery step, the programed SMP based on V-fa/PU polymer alloy at 60/40 wt% containing 7 wt% Fe_3O_4 NPs was actuated by heating to 40^{o}C, the sample was changed its shape from 3rd temporary shape to 2nd temporary shape to turn on the light on the right-hand side by completing circuit loop. After that, the sample was heated to 80 ^{o}C to change its shape from 2nd temporary shape to 1st temporary shape to turn on the light on the left-hand side. Finally, the sample SMP was then heated to 120 ^{o}C to change its shape from 1st temporary shape to original shape to turn in the middle. As demonstrated in Fig. 13, infrared temperature thermometer gun can establish that the specimen has a transient form at predetermined temperatures.

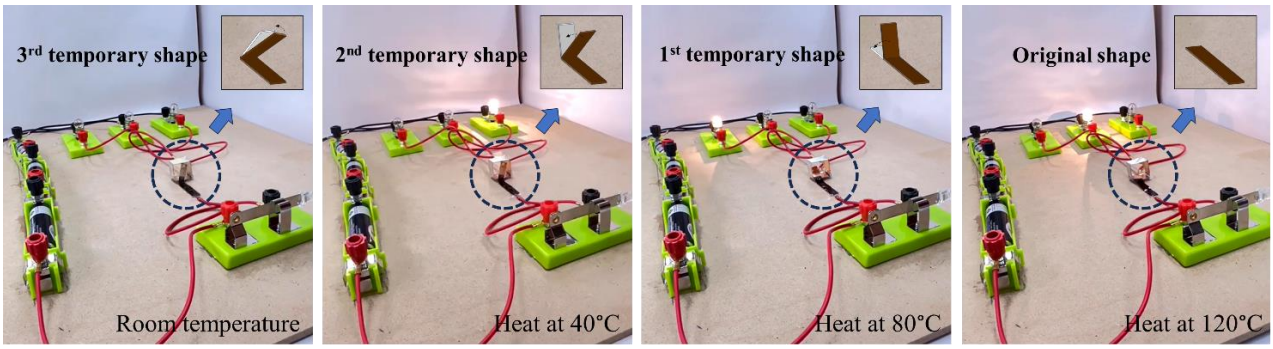

Fig. 13. Triple SMP from V-fa/PU polymer alloy incorporated by Fe_3O_4 NPs in electric circuit.

4. Conclusion

In summary, high-performance magnetic responsive triple SMPs from bio-based benzoxazine/urethane polymer alloys filled with Fe_3O_4 NPs have been successfully fabricated. The effect of PU content on shape memory performance of V-fa/PU polymer alloys was systematically studied. The results demonstrated that the incorporation of PU into polymer alloys not only increased the T_g but also generated a heterogeneous network, resulting in a broad range of T_g; a crucial feature for multiple SMPs. The results indicated that the optimal composition of V-fa/PU polymer alloys at a mass ratio of 60/40 displayed excellent shape memory ability, with shape fixity of 96 % and shape recovery of 94%. In addition, it has been shown that the magnetic properties of the Fe_3O_4 NPs-filled V-fa/PU SMPs could be efficiently induced by an external magnetic field. V-fa/PU polymer alloys with a mass ratio of 60/40 containing 7 wt% Fe_3O_4 NPs exhibited the highest shape memory performance, with shape fixity of 98%, shape recovery of 98%, and shape recovering time of 8 s. Furthermore, magnetic responsive SMP based on Fe_3O_4 NPs filled V-fa/PU polymer nanocomposites were discovered to exhibit triple shape memory behavior which can be used in electric circuit applications.

Funding

This study was funded by The National Research Council of Thailand (NRCT) and Chulalongkorn University (N42A660910) and Thailand Science Research and Innovation (TSRI) Fund Chulalongkorn University (6641/2566).

References

[1] S. Leungpuangkaew *et al.*, "Magnetic- and light-responsive shape memory polymer nanocomposites from bio-based benzoxazine resin and iron oxide nanoparticles," *Advanced Industrial and Engineering Polymer Research*, vol. 6, no. 3, pp. 215-225, 2023, doi: https://doi.org/10.1016/j.aiepr.2023.01.003.

[2] R. Sanaka and S. K. Sahu, "Influence of nanofiller addition on the mechanical, thermal, and shape recovery behavior of shape memory polymer nanocomposite: A brief review," *Materials Today: Proceedings*, 2023, doi: https://doi.org/10.1016/j.matpr.2023.06.370.

[3] M. Uyan and M. S. Celiktas, "Evaluation of the bio-based materials utilization in shape memory polymer composites production," *European Polymer Journal*, vol. 195, p. 112196, 2023, doi: https://doi.org/10.1016/j.eurpolymj.2023.112196.

[4] C. Zhang *et al.*, "From plant phenols to novel bio-based polymers," *Progress in Polymer Science*, vol. 125, p. 101473, 2022, doi: https://doi.org/10.1016/j.progpolymsci.2021.101473.

[5] S. Rouf, A. Raina, M. Irfan Ul Haq, N. Naveed, S. Jeganmohan, and A. Farzana Kichloo, "3D printed parts and mechanical properties: Influencing parameters, sustainability aspects, global market scenario, challenges and applications," *Advanced Industrial and Engineering Polymer Research*, vol. 5, no. 3, pp. 143-158, 2022, doi: https://doi.org/10.1016/j.aiepr.2022.02.001.

[6] J. Qiao, "Elastomeric nano-particle and its applications in polymer modifications," *Advanced Industrial and Engineering Polymer Research,* vol. 3, no. 2, pp. 47-59, 2020, doi: 10.1016/j.aiepr.2020.02.002.

[7] K. Friedrich, "Polymer composites for tribological applications," *Advanced Industrial and Engineering Polymer Research,* vol. 1, no. 1, pp. 3-39, 2018, doi: https://doi.org/10.1016/j.aiepr.2018.05.001.

[8] A. Karimi, D. Rahmatabadi, and M. Baghani, "Direct Pellet Three-Dimensional Printing of Polybutylene Adipate-co-Terephthalate for a Greener Future," *Polymers*, vol. 16, no. 2, doi: 10.3390/polym16020267.

[9] D. Rahmatabadi *et al.*, "4D printing of porous PLA-TPU structures: effect of applied deformation, loading mode and infill pattern on the shape memory performance," *Physica Scripta,* vol. 99, no. 2, p. 025013, 2024, doi: 10.1088/1402-4896/ad1957.

[10] C. Bo *et al.*, "Recyclable cardanol-based benzoxazines with multi-stimulus-responsive shape-memory and their carbon nanotubes composites for dynamic force sensor," *Composites Science and Technology,* vol. 230, p. 109732, 2022, doi: https://doi.org/10.1016/j.compscitech.2022.109732.

[11] P. Mora, C. Jubsilp, C.-H. Ahn, and S. Rimdusit, "Two-way thermo-responsive thermoset shape memory polymer based on benzoxazine/urethane alloys using as self-folding structures," *Advanced Industrial and Engineering Polymer Research,* vol. 6, no. 1, pp. 13-23, 2023, doi: https://doi.org/10.1016/j.aiepr.2022.09.001.

[12] S. Rimdusit, C. Jubsilp, and S. Tiptipakorn, *Alloys and Composites of Polybenzoxazines: Properties and Applications*. Springer: New York, 2013.

[13] H. Ishida and T. Agag, *Handbook of benzoxazine resins*. Amsterdam, The Netherlands: Elsevier, 2011.

[14] L. Amornkitbamrung *et al.*, "Effects of glutaric anhydride functionalization on filler-free benzoxazine/epoxy copolymers with shape memory and self-healing properties under near-infrared light actuation," *Journal of Science: Advanced Materials and Devices,* vol. 7, no. 3, p. 100446, 2022, doi: https://doi.org/10.1016/j.jsamd.2022.100446.

[15] S. Srisaard, L. Amornkitbamrung, K. Charoensuk, C. Sapcharoenkun, C. Jubsilp, and S. Rimdusit, "Effects of graphene nanoplatelets on bio-based shape memory polymers from benzoxazine/epoxy copolymers actuated by near-infrared light," *Journal of Intelligent Material Systems and Structures,* vol. 33, no. 4, pp. 547-557, 2021, doi: 10.1177/1045389X211023587.

[16] L. Amornkitbamrung, S. Srisaard, C. Jubsilp, C. W. Bielawski, S. H. Um, and S. Rimdusit, "Near-infrared light responsive shape memory polymers from bio-based benzoxazine/epoxy copolymers produced without using photothermal filler," *Polymer,* vol. 209, p. 122986, 2020, doi: https://doi.org/10.1016/j.polymer.2020.122986.

[17] S. Namathoti, R. k. V.M, and R. S. P.S, "A review on progress in magnetic, microwave, ultrasonic responsive Shape-memory polymer composites," *Materials Today: Proceedings,* vol. 56, pp. 1182-1191, 2022, doi: https://doi.org/10.1016/j.matpr.2021.11.151.

[18] T. Liu *et al.*, "Stimulus methods of multi-functional shape memory polymer nanocomposites: A review," *Composites Part A: Applied Science and Manufacturing,* vol. 100, pp. 20-30, 2017, doi: https://doi.org/10.1016/j.compositesa.2017.04.022.

[19] U. N. Kumar, K. Kratz, M. Heuchel, M. Behl, and A. Lendlein, "Shape-memory nanocomposites with magnetically adjustable apparent switching temperatures," (in eng), *Adv Mater,* vol. 23, no. 36, pp. 4157-62, 2011, doi: 10.1002/adma.201102251.

[20] C. Yakacki, N. Satarkar, K. Gall, R. Likos, and J. Hilt, "Shape-memory polymer networks with Fe3O4 nanoparticles for remote activation," *Journal of Applied Polymer Science,* vol. 112, pp. 3166-3176, 2009, doi: 10.1002/app.29845.

[21] Y. Gao, G. Zhu, S. Xu, T. Ma, and J. Nie, "Biodegradable magnetic-sensitive shape memory poly(ε-caprolactone)/Fe3O4 nanocomposites," *Journal of Applied Polymer Science,* vol. 135, 2017, doi: 10.1002/app.45652.

[22] R. Goodrum, H. Weldekidan, H. Li, A. K. Mohanty, and M. Misra, "Graphene-based nanostructures from green processes and their applications in biomedical sensors," *Advanced Industrial and Engineering Polymer Research,* 2023, doi: https://doi.org/10.1016/j.aiepr.2023.03.001.

[23] K. Mirasadi *et al.*, "3D and 4D Printing of PETG–ABS–Fe3O4 Nanocomposites with Supreme Remotely Driven Magneto-Thermal Shape-Memory Performance," *Polymers*, vol. 16, no. 10, doi: 10.3390/polym16101398.

[24] X. Wang and Z. Li, "Role of heating rate on the triple-shape memory effect of amorphous polymers: A cooperative thermodynamic model," *Polymer*, vol. 274, p. 125931, 2023, doi: https://doi.org/10.1016/j.polymer.2023.125931.

[25] H. Li *et al.*, "Dual and triple shape memory properties of poly(ε-caprolactone)-based cross-linked polymer elastomers," *Polymer Testing,* vol. 115, p. 107738, 2022, doi: https://doi.org/10.1016/j.polymertesting.2022.107738.

[26] M. Amini and S. Wu, "Designing a polymer blend nanocomposite with triple shape memory effects," *Composites Communications,* vol. 23, p. 100564, 2021, doi: https://doi.org/10.1016/j.coco.2020.100564.

[27] Y. Wang *et al.*, "Photoresponsive triple shape memory polymers with a self-healing function based on poly (lactic acid)/polycaprolactone blends," *Polymer Testing*, vol. 120, p. 107966, 2023, doi: https://doi.org/10.1016/j.polymertesting.2023.107966.

[28] T. Xie, "Tunable polymer multi-shape memory effect," *Nature*, vol. 464, no. 7286, pp. 267-270, 2010, doi: 10.1038/nature08863.

[29] P. Prathumrat, S. Tiptipakorn, and S. Rimdusit, "Multiple-shape memory polymers from benzoxazine-urethane copolymers," *Smart Materials and Structures*, Article vol. 26, no. 6, 2017, Art no. 065025, doi: 10.1088/1361-665X/aa6d47.

[30] H. Ishida, "Process for preparation of benzoxazine compounds in solventless systems, US patent no. 5543516," Patent US patent no. 5543516, 1996.

[31] W. Prasomsin, T. Parnklang, C. Sapcharoenkun, S. Tiptipakorn, and S. Rimdusit, "Multiwalled Carbon Nanotube Reinforced Bio-Based Benzoxazine/Epoxy Composites with NIR-Laser Stimulated Shape Memory Effects," *Nanomaterials*, vol. 9, p. 881, 2019, doi: https://doi.org/10.3390/nano9060881.

[32] A. Van, K. Chiou, and H. Ishida, "Use of renewable resource vanillin for the preparation of benzoxazine resin and reactive monomeric surfactant containing oxazine ring," *Polymer*, vol. 55, no. 6, pp. 1443-1451, 2014, doi: 10.1016/j.polymer.2014.01.041.

[33] R. Liu *et al.*, "Castor oil-based polyurethane networks containing diselenide bonds: Self-healing, shape memory, and high flexibility," *Progress in Organic Coatings*, vol. 163, p. 106615, 2022, doi: https://doi.org/10.1016/j.porgcoat.2021.106615.

[34] T. Parnklang, K. Boonyanuwat, P. Mora, S. Ekgasit, and S. Rimdusit, "Form-stable benzoxazine-urethane alloys for thermally reversible light scattering materials," (in English), *Express Polym. Lett.*, vol. 13, pp. 65-83, 2019, doi: https://doi.org/10.3144/expresspolymlett.2019.7.

[35] S. Rimdusit, S. Tiptipakorn, C. Jubsilp, and Takeichi, "Polybenzoxazine alloys and blends: Some unique properties and applications," *Reactive and Functional Polymers,* vol. 73, pp. 369–380, 2013, doi: 10.1016/j.reactfunctpolym.2012.04.022.

[36] T. Takeichi, Y. Guo, and T. Agag, "Synthesis and characterization of poly(urethane-benzoxazine) films as novel type of polyurethane/phenolic resin composites," *Journal of Polymer Science Part A: Polymer Chemistry,* vol. 38, pp. 4165-4176, 2000, doi: 10.1002/1099-0518(20001115)38:22<4165::AID-POLA170>3.0.CO;2-S.

[37] P. Mora, C. Jubsilp, C. W. Bielawski, and S. Rimdusit, "Impact Response of Aramid Fabric-Reinforced Polybenzoxazine/Urethane Composites Containing Multiwalled Carbon Nanotubes Used as Support Panel in Hard Armor," (in eng), *Polymers (Basel),* vol. 13, no. 16, 2021, doi: https://doi.org/10.3390/polym13162779.

[38] S. Rimdusit, M. Sudjidjune, C. Jubsilp, and S. Tiptipakorn, "Enhanced Film Forming Ability of Benzoxazine- Urethane Hybrid Polymer Network by Sequential Cure Method," *Journal of Applied Polymer Science,* vol. 131, 2014, doi: 10.1002/app.40502.

[39] B.-X. Cheng *et al.*, "A review of microphase separation of polyurethane: Characterization and applications," *Polymer Testing,* vol. 107, p. 107489, 2022, doi: https://doi.org/10.1016/j.polymertesting.2022.107489.

[40] S. Li, J. Zhang, C. Jianjun, Y. Ming, L. Xuepeng, and J. Zhiguo, "Biodegradable body temperature-responsive shape memory polyurethanes with self-healing behavior," *Polymer Engineering & Science,* vol. 59, pp. E310-E316, 2019, doi: https://doi.org/10.1002/pen.25061.

[41] C. Wang, Z. Li, G. Lu, H. Zhen, Y. Liu, and M. Run, "Synthesis, Dynamic Mechanical Properties, and Shape Memory Effect of Poly(benzoxazine-ether-urethane)s," *ChemistrySelect,* vol. 6, pp. 2539-2547, 2021, doi: 10.1002/slct.202100307.

[42] L. Li, B. Zhao, H. Wang, Y. Gao, J. Hu, and S. Zheng, "Nanocomposites of polyhydroxyurethane with Fe3O4 nanoparticles: Synthesis, shape memory and reprocessing properties," *Composites Science and Technology,* vol. 215, p. 109009, 2021, doi: https://doi.org/10.1016/j.compscitech.2021.109009.

[43] K. Kim, S. S. Kim, Y.-H. Choa, and H. T. Kim, "Formation and surface modification of Fe3O4 nanoparticles by co-precipitation and sol-gel method," *J. Ind. Eng. Chem.*, vol. 13, pp. 1137-1141, 2007.

[44] S. Chaki, T. Malek, M. Chaudhary, J. Tailor, and M. Deshpande, "Magnetite Fe 3 O 4 nanoparticles synthesis by wet chemical reduction and their characterization," *Advances in Natural Sciences: Nanoscience and Nanotechnology*, vol. 6, 2015, doi: 10.1088/2043-6262/6/3/035009.

[45] H. Kalita and N. Karak, "Biobased Hyperbranched Shape-Memory Polyurethanes: Effect of Different Vegetable Oils," *Journal of Applied Polymer Science*, vol. 131, 2014, doi: 10.1002/app.39579.

[46] G. D. Soto, C. Meiorin, D. Actis, P. Mendoza Zélis, M. A. Mosiewicki, and N. E. Marcovich, "Nanocomposites with shape memory behavior based on a segmented polyurethane and magnetic nanostructures," *Polymer Testing*, vol. 65, pp. 360-368, 2018, doi: https://doi.org/10.1016/j.polymertesting.2017.12.012.

[47] C. Likitaporn, P. Mora, S. Tiptipakorn, and S. Rimdusit, "Recovery stress enhancement in shape memory composites from silicon carbide whisker–filled benzoxazine-epoxy polymer alloy," *Journal of Intelligent Material Systems and Structures,* vol. 29, no. 3, pp. 388-396, 2017, doi: 10.1177/1045389X17708041.

[48] H. Kalita and N. Karak, "Hyperbranched polyurethane/Fe3O4 thermosetting nanocomposites as shape memory materials," *Polymer Bulletin,* vol. 70, no. 11, pp. 2953-2965, 2013, doi: 10.1007/s00289-013-0999-8.

[49] A. Golbang and M. Kokabi, "Temporary shape development in shape memory nanocomposites using magnetic force," *European Polymer Journal,* vol. 47, no. 8, pp. 1709-1719, 2011, doi: https://doi.org/10.1016/j.eurpolymj.2011.06.008.

[50] H. Kalita, (Shape Memory Polymers). Berlin, Boston: De Gruyter, 2018.

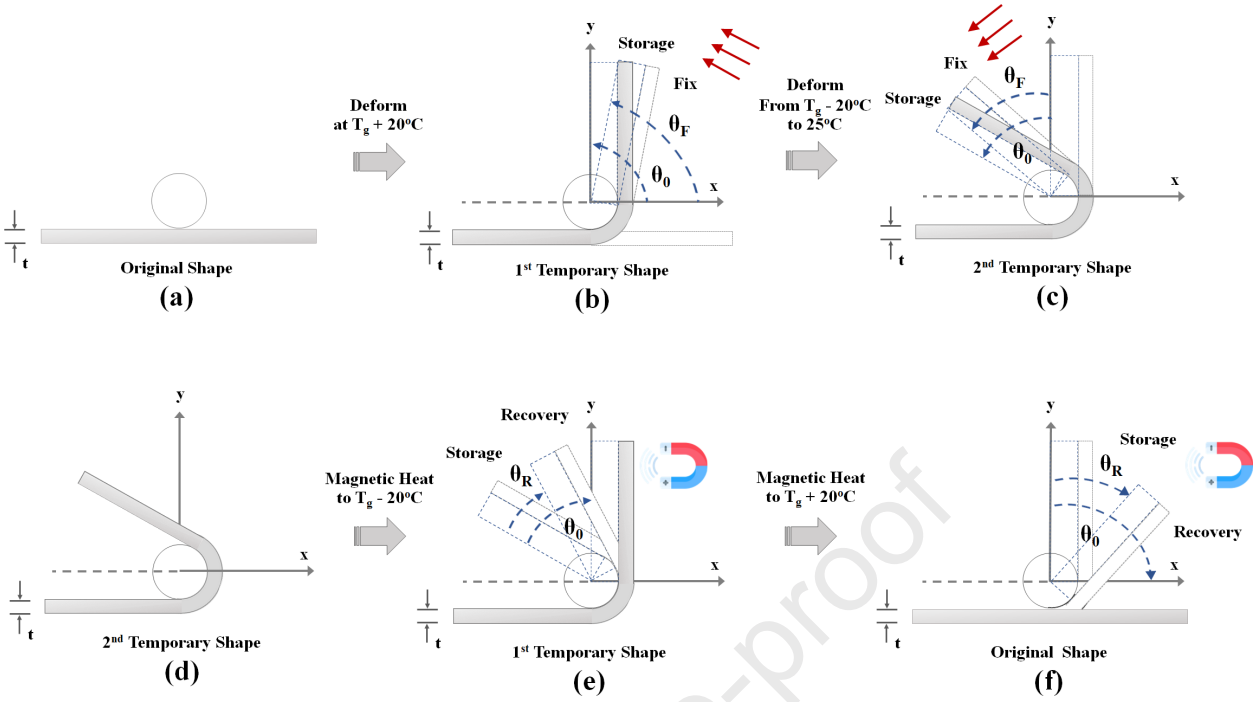

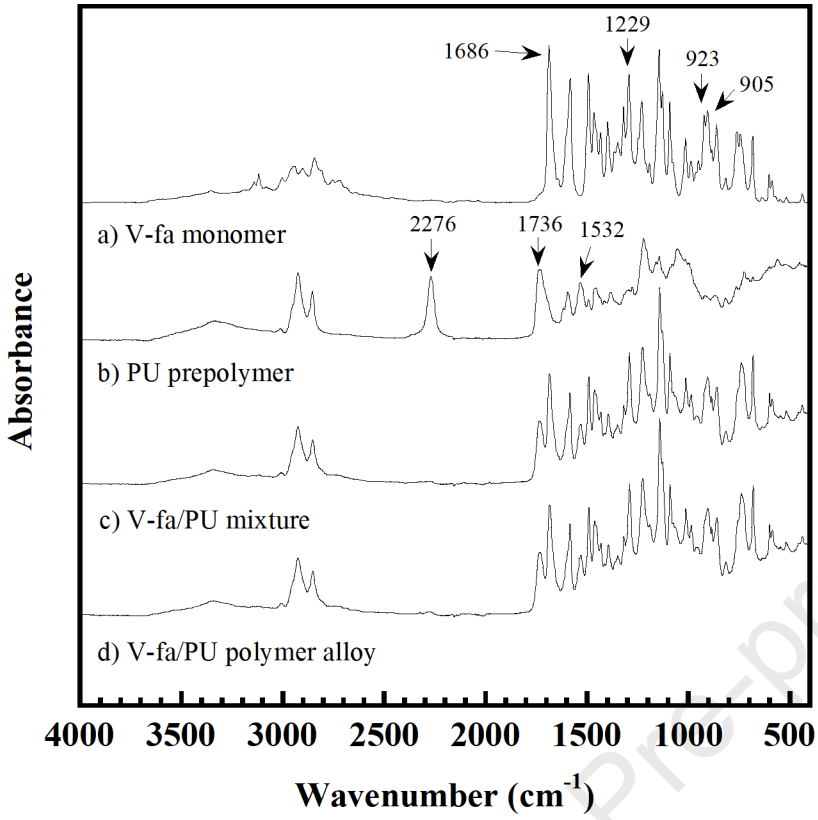

a)

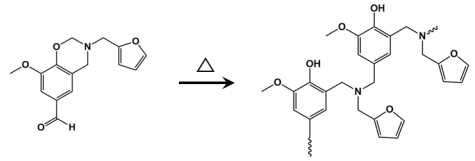

V-fa Poly(V-fa)

b)

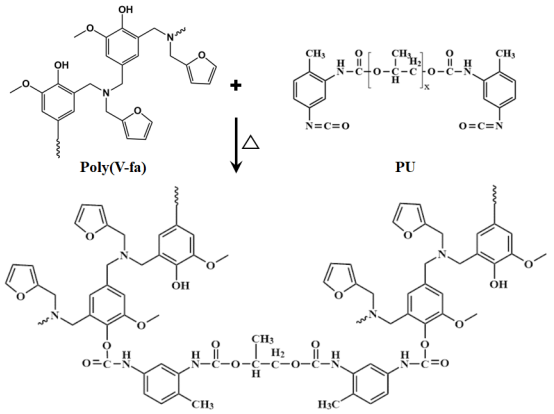

Poly(V-fa) PU

V-fa/PU polymer alloy